The Astrophysical Journal, 661:1013–1024, 2007 June 1

ON THE PROGENITORS OF TWO TYPE II-P SUPERNOVAE IN THE VIRGO CLUSTER[1,2]

Weidong Li,[3] Xiaofeng Wang,[3,4] Schuyler D. Van Dyk,[5] Jean-Charles Cuillandre,[6]
Ryan J. Foley,[3] and Alexei V. Filippenko[3]
Received 2007 January 2; accepted 2007 February 14

ABSTRACT

Direct identification of the progenitors of supernovae (SNe) is rare because of the required spatial resolution and depth of the archival data prior to the SN explosions. Here we report on the identification of the progenitors of two nearby SNe in the Virgo Cluster: SN 2006my in NGC 4651 and SN 2006ov in M61. We obtained high-quality ground-based images of SN 2006my with the Canada-France-Hawaii Telescope, and are able to locate the site of the SN on pre-SN *Hubble Space Telescope* (*HST*) Wide Field Planetary Camera 2 images to a high precision (1 σ uncertainty of $\pm 0.05''$). We pinpoint the site of SN 2006ov to within $0.02''$ from *HST* Advanced Camera for Surveys images of the SN. We detected a red supergiant progenitor for each SN within the error circles, with an inferred zero-age main-sequence mass ($M_{\rm zams}$) of 10^{+5}_{-3} and 15^{+5}_{-3} $M_\odot$ for the progenitors of SNe 2006my and 2006ov, respectively. The mass estimates for the progenitors of both SNe confirm a suggested trend that the most common Type II–plateau SNe originate from low-mass supergiants with $M_{\rm zams} \approx 8$–20 $M_\odot$.

Subject headings: supernovae: general — supernovae: individual (SN 2006my, SN 2006ov) — stars: evolution

1. INTRODUCTION

When a bright, nearby supernova (SN) is discovered, it may be possible to directly identify the progenitor of the SN in deep pre-SN images. Analysis of the properties (e.g., mass, spectral type) of such SN progenitors allows a direct comparison to theoretical expectations based on the observed quantities of the SNe (e.g., light curves, spectral evolution).

While observers have had some luck with ground-based observations, such as the identifications of a $\sim$20 $M_\odot$ blue supergiant (BSG) star for the peculiar, subluminous Type II SN 1987A in the Large Magellanic Cloud (Gilmozzi et al. 1987; Sonneborn et al. 1987), a $\sim$17 $M_\odot$ red supergiant (RSG), possibly in a binary system, for the Type IIb SN 1993J in M81 (Aldering et al. 1994; Van Dyk et al. 2002), and a 13–20 $M_\odot$ yellow supergiant (YSG) for the Type II-P SN 2004et in NGC 6946 (Li et al. 2005a, 2005b), most of the recent progress in this field has been based on the rich archival data of the *Hubble Space Telescope* (*HST*) (Van Dyk et al. 2003a; Smartt et al. 2004; Maund & Smartt 2005; Maund et al. 2005a; Li et al. 2006; Hendry et al. 2006; Gal-Yam et al. 2007). The superior spatial resolution of the *HST* images allows the SN progenitors to be isolated from their environments, and the deep limiting magnitude allows the SN progenitors to be detected in more distant (but still relatively nearby) galaxies.

In this paper we report the identification of the progenitors on *HST* images of two nearby SNe in the Virgo Cluster. K. Itagaki, a veteran Japanese amateur SN searcher, discovered both of these SNe: SN 2006my in NGC 4651 on 2006 November 8.82 (UT dates are used throughout this paper) and SN 2006ov in M61 (NGC 4303) on 2006 November 24.86 (Nakano & Itagaki 2006a, 2006b). Unfortunately, the SN explosions occurred while the galaxies were behind the Sun, and were only detected after becoming visible again in the early morning, so the objects were discovered rather late in their evolution. Spectra obtained soon after the time of discovery show that both SNe are of Type II: SN 2006my is similar to SN II-P 1999em (Hamuy et al. 2001; Leonard et al. 2002b; Elmhamdi et al. 2003) about 1–2 months after maximum brightness (Stanishev & Nielsen 2006), and SN 2006ov, perhaps reddened, is similar to SN II-P 2005cs (Pastorello et al. 2006; Takáts & Vinkó 2006) roughly a month after maximum (Blondin et al. 2006) (see § 2 for a more detailed discussion of the age and reddening of both SNe).

We took ground-based images of the SNe with the Canada-France-Hawaii Telescope (CFHT) under good seeing conditions (Figs. 1 and 2), and are able to precisely (to within $\sim 0.05''$ and $0.11''$, for SNe 2006my and 2006ov, respectively) locate the site of both SNe on pre-SN archival *HST* images of the host galaxies. We further obtained *HST* ACS images of SN 2006ov itself and were able to pinpoint the SN site to within $0.02''$. We identify a 7–15 $M_\odot$ red supergiant (RSG) and a 12–20 $M_\odot$ RSG in the error circles of SNe 2006my and 2006ov, respectively, and propose these as the progenitors of the SNe. We note that NGC 4651 also produced SN 1987K, while M61 produced SNe 1926A, 1961I, 1964F, and 1999gn.

This paper is organized as follows. In § 2 we discuss the properties (type, age, and reddening) of both SNe, and demonstrate that they are of the Type II variety discovered near the end of the plateau phase. In § 3 we report our identification of the progenitors in the pre-SN *HST* WFPC2 images. We describe the nature of the progenitors inferred from the *HST* photometry in § 4. Further discussion is in § 5, and we summarize our conclusions in § 6.

2. OBSERVATIONS OF SN 2006my AND SN 2006ov

There are several subclasses of SNe II (see Filippenko 1997 for a review of SN types). Among these, the Type II–plateau SNe

[1] Based on observations made with the NASA/ESA *Hubble Space Telescope*, obtained at the Space Telescope Science Institute, which is operated by the Association of Universities for Research in Astronomy, Inc., under NASA contract NAS 5-26555. These observations are associated with program GO-10877.

[2] Based on observations obtained with MegaPrime/MegaCam, a joint project of CFHT and CEA/DAPNIA, at the Canada-France-Hawaii Telescope (CFHT), which is operated by the National Research Council (NRC) of Canada, the Institute National des Sciences de l'Univers of the Centre National de la Recherche Scientifique of France, and the University of Hawaii.

[3] Department of Astronomy, University of California, Berkeley, CA 94720-3411.

[4] Tsinghua Center for Astrophysics (THCA) and Physics Department, Tsinghua University, Beijing, 100084, China.

[5] *Spitzer* Science Center, California Institute of Technology, Pasadena, CA 91125.

[6] Canada-France-Hawaii Telescope Corporation, Kamuela, HI 96743.

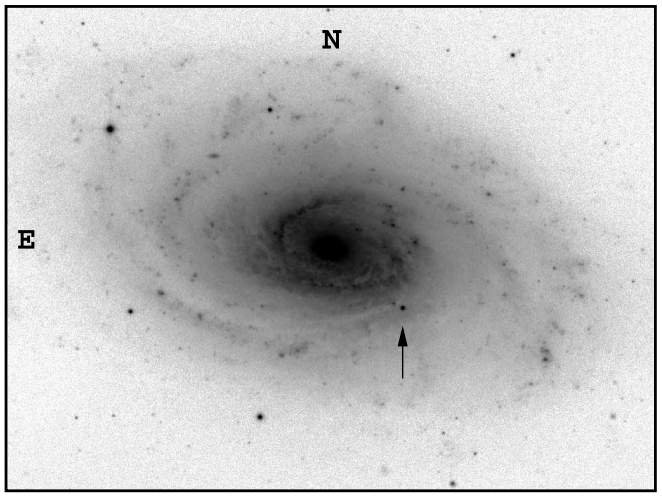

FIG. 1.—A $4' \times 3'$ section of the CFHT r'-band MegaCam image of SN 2006my, taken under $0.6''$ seeing on 2006 December 24. SN 2006my is marked with an arrow.

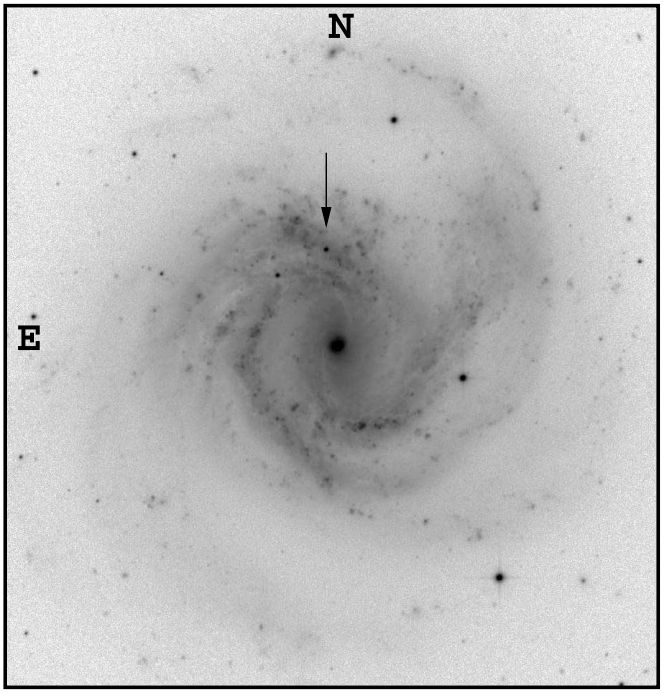

FIG. 2.—A $6' \times 6'$ section of the CFHT r'-band MegaCam image of SN 2006ov, taken under $1.0''$ seeing on 2006 November 27. SN 2006ov is marked with an arrow.

(SNe II-P) are the most common, with the defining feature being a prominent plateau phase in their optical light curve. The Type II–linear SNe (SNe II-L) show a linear decline in magnitude after their maximum brightness, and are relatively rare. The SN 1987A–like objects are subluminous and show a very broad peak in the light curve. The Type II–narrow SNe (SNe IIn), which have relatively narrow spectral features sometimes (but not always) superimposed on a broader component, are a more heterogeneous subclass than the others. Moreover, the Type IIb SNe, such as SN 1993J in M81 (Filippenko et al. 1993; Nomoto et al. 1993), manifest themselves as SNe II at early times, but then experience a spectroscopic metamorphosis into a SN Ib at late times (see SN 1987K, Filippenko 1988).

The different subclasses may have quite different progenitor systems. Thus in this section, we study the photometric and spectroscopic behavior of SNe 2006my and 2006ov, to get an initial indication of their nature.

2.1. *Photometry of SN 2006my and SN 2006ov*

We followed SNe 2006my and 2006ov with the 0.76 m Katzman Automatic Imaging Telescope (KAIT; Li et al. 2000; Filippenko et al. 2001; Filippenko 2005) at Lick Observatory soon after their discoveries. KAIT, which conducts the successful Lick Observatory Supernova Search (LOSS), did not discover these two SNe because of its search strategy of focusing on near-meridian objects, and the two SNe were 2–3 hr east of the meridian at the end of the night when discovered by Itagaki. As both SNe were discovered at late times, we did not start an intense multicolor campaign of follow-up observations. Instead, the two SNe were imaged in unfiltered mode nearly nightly, with occasional broadband *BVRI* photometry.

An advantage of observing with the unfiltered mode is that we have good pre-SN unfiltered template images for the SN host galaxies accumulated during the course of LOSS. These templates enable us to perform galaxy subtraction, which significantly increases the photometric accuracy as both SNe (especially SN 2006ov) are heavily contaminated by host-galaxy emission. Here we report relative unfiltered photometry for SNe 2006my and 2006ov, providing the necessary information on their photometric behavior (e.g., whether they have a plateau or linear phase). A full treatment of all available follow-up data for these SNe is beyond the scope of this paper, and will be discussed elsewhere.

For the unfiltered images of SNe 2006my and 2006ov, we first perform galaxy subtraction with a customized software package. The SN image is registered to the pre-SN unfiltered template, their point-spread functions (PSFs) are convolved to the same level, the intensities of the images are matched, and a final subtraction is performed. This procedure is essentially that used for processing unfiltered images by the LOSS SN search pipeline. We use the IRAF[7] DAOPHOT package (Stetson 1987) to perform standard aperture photometry for the SNe and several bright stars in the field. A relative light curve is then generated by averaging the differences between the magnitudes of the SNe and the bright stars.

As the best match to broadband filters for the KAIT unfiltered data is the *R* band (Li et al. 2003), in Figure 3 we compare our relative unfiltered light curves for SNe 2006my and 2006ov to the *R*-band light curve of SN 1999em, a well-studied SN II-P (Leonard et al. 2002b; Hamuy et al. 2001; Elmhamdi et al. 2003). The relative unfiltered light curves of the SNe are visually shifted by a constant to match the light curve of SN 1999em. Figure 3 indicates a good match between SN 1999em and SN 2006my: the behavior of the decline from the plateau is almost identical for both SNe. There is no doubt that SN 2006ov is a SN II-P as well, because it shows a prominent plateau phase. However, it has a steeper decline from the plateau than do SNe 1999em and 2006my.

Thus, SN 2006my and SN 2006ov behave like SNe II-P discovered near the end of their plateau phase. The duration of the plateau phase of SNe II-P, however, varies significantly. From a sample of 13 SNe II-P studied by Hamuy (2003), Hendry et al. (2005) derived a mean plateau duration of 131 ± 21 days, with a range of 110–170 days. Consequently, it is unclear which SN

[7] IRAF (Image Reduction and Analysis Facility) is distributed by the National Optical Astronomy Observatory, which is operated by the Association of Universities for Research in Astronomy, Inc., under cooperative agreement with the National Science Foundation.

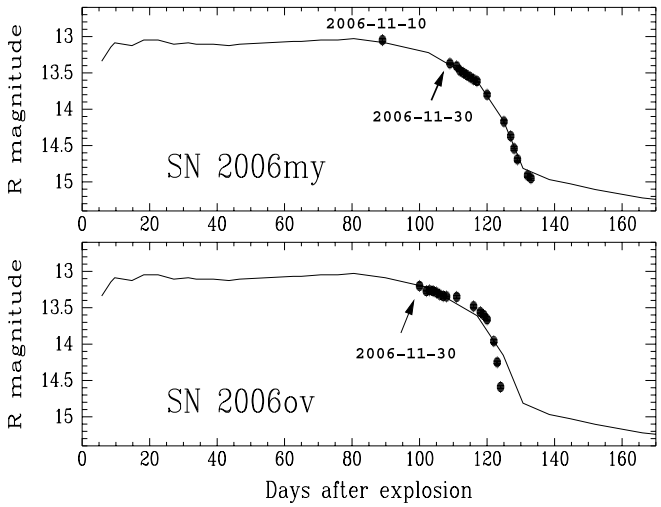

FIG. 3.—Comparison of the light curves of SNe 2006my and 2006ov to that of SN 1999em (Hamuy et al. 2001; Leonard et al. 2002b). The photometry of SNe 2006my and 2006ov was performed on unfiltered images, and the data were visually shifted by a constant to match SN 1999em (whose light curve is plotted as a solid line). Dates of some observations are marked. Both SNe show characteristics of SNe II-P discovered near the end of the plateau phase.

exploded first, SN 2006my or SN 2006ov. Although SN 2006my appears to be farther along the plateau than SN 2006ov on the same date, SN 2006ov could have had a longer plateau phase and thus exploded earlier.

Our estimate of the age of SNe 2006my and 2006ov at the time of discovery ($\sim$3 months after explosion) is somewhat older than the ages suggested by other groups based on spectra: $\sim$1–2 months for SN 2006my (Stanishev & Nielsen 2006), and $\sim$1 month for SN 2006ov (Blondin et al. 2006). Next, we will check our own spectra to provide further age estimates for both SNe, and attempt to constrain the reddening toward them.

2.2. *Spectroscopy of SN 2006my and SN 2006ov*

We obtained three optical spectra of SNe 2006my and 2006ov with the Keck 10 m telescopes using the Low Resolution Imaging Spectrometer (LRIS; Oke et al. 1995), and with the Lick Observatory 3 m Shane Telescope using the Kast double spectrograph (Miller & Stone 1993). A journal of observations is given in Table 1. All one-dimensional sky-subtracted spectra were extracted optimally in the usual manner (e.g., Foley et al. 2003). For the Kast observations, flat fields for the red-side CCD were taken at the position of the object to reduce near-infrared fringing effects. The spectra were corrected for atmospheric extinction and telluric bands (Bessell 1999; Matheson 2000), and then flux-calibrated using standard stars observed at similar air mass on the same night as the SNe.

In Figure 4 we show a comparison of the spectra of SNe 2006my and 2006ov to those of other well-studied SNe II-P at similar epochs. The spectra of SNe 2004dj and 2003gd are previously unpublished data from our own spectral database. All spectra in Figure 4 have been corrected for the reddening toward the SNe and also for the host-galaxy redshift. For SN 2003gd, we adopt $E(B-V) = 0.13$ mag, and an explosion date of 2003 March 17 (Van Dyk et al. 2003c). For SN 2004dj, we adopt $E(B-V) = 0.07$ mag, and an explosion date of 2004 June 30 (Zhang et al. 2006; Vinkó et al. 2006). We emphasize that both SNe 2003gd and 2004dj were discovered in the middle of the plateau phase, so their explosion dates have relatively large uncertainties due to the large scatter in the plateau durations. Only the Galactic reddenings of $E(B-V) = 0.027$ and 0.022 mag (Schlegel et al. 1998) were removed from the spectra of SN 2006my and SN 2006ov, respectively.

Figure 4 demonstrates a striking similarity between the spectra of SN 2006my and SN 2006ov, as well as their resemblance to the spectra of SNe 2004dj and 2003gd at 3–4 months after explosion. Other signs of a relatively old age for these SNe II-P are the strong, relatively narrow, Ca II near-IR triplet (one sees the 8498 and 8662 Å components, with the 8542 Å component blended within), and hints of the [Ca II] $\lambda\lambda$7291, 7324 and [Fe II] λ7155 lines often seen in SNe II-P during the nebular phase.

The spectra in Figure 4 also show that with just the corrections for Galactic reddening, the spectra of SNe 2006my and 2006ov have a continuum shape similar to that of the other two SNe II-P. This argues against the existence of large host-galaxy reddening toward either SN 2006my or SN 2006ov. Blondin et al. (2006), however, suggested that SN 2006ov is reddened (but they did not quote an estimate of the amount of the host-galaxy reddening). A possible cause of this discrepancy may be that Blondin et al. compared their spectrum of SN 2006ov to that of a SN II-P at a much earlier phase ($\sim$1 month after explosion) than our estimated age ($\sim$3 months after explosion). As SNe II-P become progressively redder at later times, comparing the spectrum of an older SN II-P to a younger object would give the incorrect impression that the older object is reddened.

To further investigate the reddening, in Figure 5 we plot a close-up of the spectral range near the Na I D absorption lines of both SN 2006my and SN 2006ov. It is expected that reddening caused by the dust in a galaxy would produce noticeable narrow Na I D absorption lines in an object's spectrum, although the quantitative correlation between the strength of Na I D absorption and the amount of reddening is still quite uncertain. Figure 5 shows no signs of prominent, narrow Na I D at the rest wavelengths corresponding to either the Milky Way Galaxy or the hosts (a hint of narrow Na I D absorption due to the Milky Way Galaxy might be present in the spectrum of SN 2006ov). We conclude that there is no evidence for significant host-galaxy reddening of either SN 2006my and SN 2006ov.

TABLE 1
JOURNAL OF SPECTROSCOPIC OBSERVATIONS OF SNe 2006my AND 2006ov

SN	UT Date	t_{disc}[a]	Telescope	Instrument	Range[b] (Å)	Air Mass[c]	Slit (arcsec)	Exposure Time (s)
2006my	2006 Nov23	15	Keck I 10 m	LRIS	3086–9250	1.55	1.0	200
2006my	2006 Dec 01	23	Lick 3 m	Kast	3310–10400	1.25	2.0	1500
2006ov.....	2006 Dec 01	7	Lick 3 m	Kast	3310–10400	1.48	2.0	1500

[a] Time in days since discovery.
[b] Observed wavelength range of spectrum.
[c] Average air mass of observations.

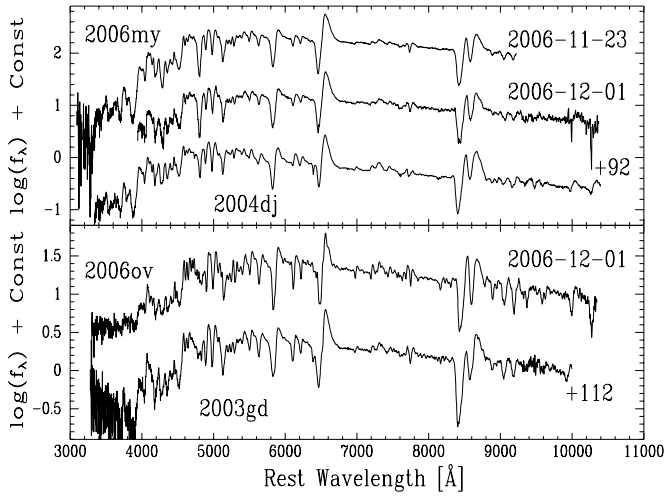

FIG. 4.—Comparison of the spectra of SNe 2006my and 2006ov to those of other well-studied SNe II-P at similar epochs. The spectra have been corrected for reddening and host-galaxy redshift (see text for details).

The photometry and spectroscopy of SNe 2006my and 2006ov indicate that both objects are SNe II-P discovered near the end of the plateau phase. We now turn to the analysis of the archival *HST* data available for NGC 4651 and M61, identifying the progenitors of both SNe and studying the environments of the progenitors.

3. THE PROGENITORS OF SNe 2006my AND 2006ov IN ARCHIVAL *HST* IMAGES

Tables 2 and 3 list the pre-SN archival *HST* WFPC2 data available for the host galaxies of SN 2006my (NGC 4651) and SN 2006ov (M61). There are also STIS, NICMOS, and ACS/HRC data for M61, but the actual site of SN 2006ov was not observed in those cases. For the *HST* WFPC2 data, the site of SN 2006my was imaged in the F555W and F814W filters (Table 2), while the site of SN 2006ov was imaged in the F450W, F606W, and F814W filters (Table 3). (Hereafter, we will refer to these images by their filter names.) We downloaded the *HST* WFPC2 data for NGC 4651 and M61 from the *HST* Multimission Archive,[8] and analyzed them with the STSDAS software package. Cosmic-ray hits in the CR-split images were removed using the task CRREJ, and the images on the four individual WFPC2 chips were combined in a mosaic using the task WMOSAIC.

[8] See http://archive.stsci.edu.

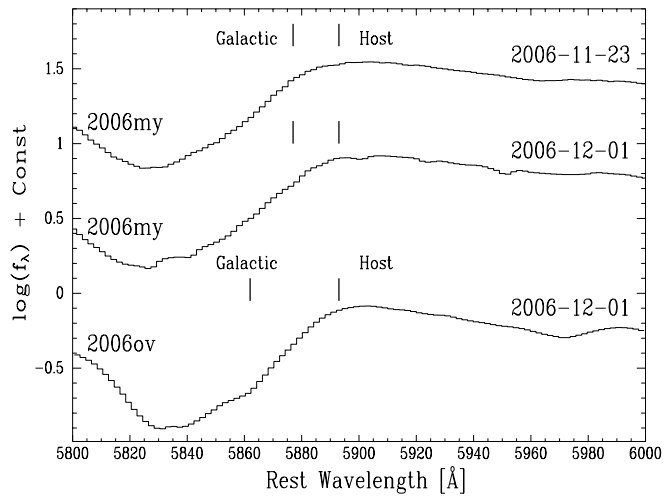

FIG. 5.—Close-up of the spectra of SNe 2006my and 2006ov. The expected positions of the interstellar Na I D absorption lines at the rest wavelength (Galactic lines) and at the redshift of the SN (host-galaxy lines) are marked. No apparent Na I D absorption lines due to the host galaxies are observed.

TABLE 2
HST WFPC2 DATA FOR NGC 4651 PRE-SN 2006my

Data Set	UT Date	Exposure Time (s)	Filter	Proposal ID
u2dt0901t	1994 May 20	60	F555W	5375
u2dt0903t	1994 May 20	300	F555W	5375
u2dt0903t	1994 May 20	300	F555W	5375
u2dt0904t	1994 May 20	60	F814W	5375
u2dt0905t	1994 May 20	300	F814W	5375
u2dt0906t	1994 May 20	300	F814W	5375
u2ex0f01t[a]	1995 Mar 4	900.0	F218W	5419
u2ex0f02t[a]	1995 Mar 4	900.0	F218W	5419
u2ex0f03t[a]	1995 Mar 4	300.0	F547M	5419

[a] The site of SN 2006my was not imaged.

It is essential to locate with high astrometric precision the SN sites in the pre-SN *HST* WFPC2 images. For this purpose, we obtained high-resolution ($0.187''$ pixel^{-1}) images of SNe 2006my and 2006ov with the 3.6 m Canada-France-Hawaii Telescope (CFHT + MegaCam) in the Sloan r' band under fair to excellent seeing conditions (FWHM intensity about $0.6''-1.0''$). A summary of these CFHT data is given in Table 4.

3.1. *Astrometric Solution for NGC 4651 and SN 2006my*

We attempted to match the CFHT r'-band images of SN 2006my to the mosaic F814W image of NGC 4651. Both sets of CFHT images give consistent results, and here we present the results from the 2006 December 24 image due to its superior depth and seeing. We identified 20 stars (or compact star clusters) present in both the CFHT and WFPC2 images for which we were able to precisely measure the (X, Y) center positions. Then, using the IRAF task GEOMAP, we performed a geometrical transformation between the two sets of coordinates, and were able to match them to $\lesssim 0.98$ WFC pixel root-mean-square ($1\ \sigma \lesssim 0.098''$). As the mosaic process involves some uncertainties caused by geometrical distortions and chip gaps among the four individual WFPC2 chips, we further attempted to match the CFHT image to the Chip 2 (WFC2) F814W image (where the SN site is located) before the image was mosaicked. Thirteen common stars were identified, with a geometrical transformation uncertainty of 0.45 pixel ($1\ \sigma \lesssim 0.045''$).

The SN position measured on the CFHT image was then transformed to the WFPC2 image. The transformed SN locations based

TABLE 3
HST WFPC2 DATA FOR M61 PRE-SN 2006ov

Data Set	UT Date	Exposure Time (s)	Filter	Proposal ID
u29r4d01t	1994 Jun 6	80	F606W	5446
u29r4d02t	1994 Jun 6	80	F606W	5446
u33z0801t[a]	1996 Mar 15	600	F218W	6358
u33z0802t[a]	1996 Mar 15	600	F218W	6358
u6ea6201r	2001 Jul 26	230	F450W	9042
u6ea6202r	2001 Jul 26	230	F450W	9042
u6ea6203r	2001 Jul 26	230	F814W	9042
u6ea6204r	2001 Jul 26	230	F814W	9042

[a] The site of SN 2006ov was not imaged.

TABLE 4
SUMMARY OF CFHT MEGACAM OBSERVATIONS

SN	UT Date	Filter	Exposure Time (s)	Pixel Scale (arcsec)	Seeing (arcsec)
2006my	2006 Nov 19	r'	60	0.185	0.8
2006my	2006 Dec 24	r'	60×5	0.185	0.6
2006ov.....	2006 Nov 27	r'	48×5	0.185	1.0

on the geometrical transformation using the mosaic image and the individual WFC2 image are consistent with each other within the uncertainties, and we adopt the SN location based on the WFC2 chip image.

Figure 6 shows a $5'' \times 5''$ close-up of the SN 2006my environment in the WFPC2 images (the F555W image has the same pointing as the F814W image). The white circles in Figure 6 have a radius of $0.225''$ (5×1 σ error). Within the 1 σ error circle, there is an apparent source in the F814W image, but no apparent point sources are visible in the F555W image. Figure 6 also shows the images with a resampled resolution of $0.05''$ pixel^{-1} (a cubic spline function is used to interpolate one pixel into 2×2 pixels). As can be seen, resampling the data brings out more details in the undersampled WFPC2 data, and the red source within the error radius of the F814W image is more easily discerned. We note that resampling the data has the risk of smoothing several (extended) sources into a point source, but in this case the point source is apparent in the original image as well.

In both the original and the resampled images, the source appears to have a slight east-west extension. It is unclear whether this source is actually a blending of two stars, given the relatively low signal-to-noise ratio (S/N) for the detection, and given the low spatial resolution of *HST* WFPC2 at the distance of NGC 4651. The probability of two RSGs occurring in adjacent pixels on the

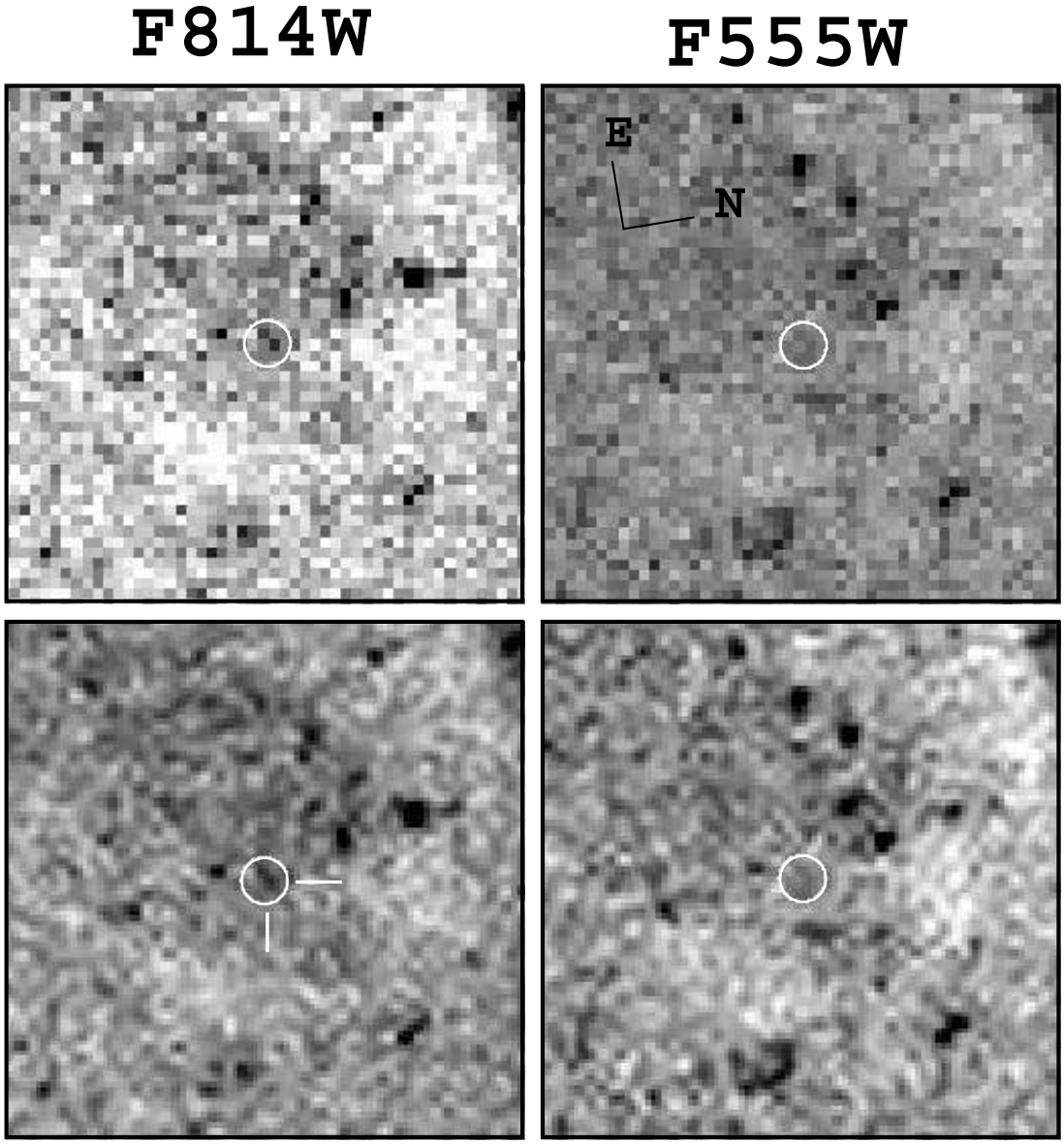

FIG. 6.—A $5'' \times 5''$ close-up of the SN 2006my environment in the *HST* WFPC2 F814W and F555W images. The white circles mark 5 times the 1 σ uncertainty of the astrometric registration. The top panel shows the images in the original WFPC2 resolution ($0.1''$ pixel^{-1}), while the bottom panel resamples the data to a resolution of $0.05''$ pixel^{-1} to bring out more details. The candidate progenitor is marked by a cross hair in the resampled F814W image. Photometry of the stars was performed on the original images.

TABLE 5
HST ACS Observations of SN 2006ov

Data Set[a]	UT Date	Exposure Time (s)	Filter	Proposal ID
j9nw50011.....	2006 Dec 12	420	F435W	10877
j9nw50021.....	2006 Dec 12	180	F625W	10877

[a] The site of SN 2006ov was not imaged.

WFC2 image, however, is very small considering the density of such stars in the environment of SN 2006my (0.4%, not including possible physical clustering of massive stars; see discussion in § 5). We consider this source as a single star, and the likely progenitor of SN 2006my. The nature of this source is further discussed in § 4.

In the original non-mosaic *HST* WFPC2 images, the SN site is located at $(X, Y) = (410.61, 158.81)$ on Chip 2 (WFC2), with a 1 σ error circle radius of 0.45 pixel. We note that these coordinates are in the IRAF system, and need to be adjusted in some other software packages. For example, the photometry packages Dophot and HSTphot use a coordinate system that differs from that of IRAF by 0.5 pixel in both *X* and *Y*. In HSTphot, which we use to reduce the *HST* WFPC2 data in this paper, the SN site is located at $(X, Y) = (410.11, 158.31)$ on the WFC2 chip.

3.2. *Astrometric Solution for M61 and SN 2006ov*

We first attempted an astrometric solution for M61 and SN 2006ov between the CFHT and the pre-SN *HST* WFPC2 F814W images. Twenty-five common stars were used in IRAF/GEOMAP to do a geometrical transformation with a precision of 1 $\sigma \lesssim$ 1.10 WFC pixel (0.11″), due to the mediocre seeing of the CFHT image. Nontheless, after mapping the SN position from the CFHT image onto the pre-SN F814W image, we identified a possible progenitor within the 1 σ error radius, which is subsequently verified by the better astrometric solution described below.

To further improve the astrometric solution, we took images of SN 2006ov with *HST* ACS on 2006 December 12, as part of SNAP program GO-10877 (PI: W. Li). The details of the observations are listed in Table 5. The ACS images were observed with the High Resolution Channel (HRC) of ACS with a spatial resolution of 0.025″ pixel^{-1} and a field of view of 29″ × 25″. We identified 12 common stars in the ACS/HRC F625W image and the Chip 4 (WFC4) pre-SN WFPC2 F814W image (where the SN site is located), and achieved an astrometric solution with a 1 σ error of 0.17 WFC pixel (0.017″) (Fig. 7). The F450W image has the same pointing as the F814W image, but the F606W image does not. An astrometric solution between the ACS/HRC F625W image and the Chip 4 (WFC4) WFPC2 F606W image (where the SN site is located) using nine common stars yields a precision with a 1 σ uncertainty of 0.16 WFC pixel (0.016″). Using these astrometric solutions, the SN position measured in the ACS/HRC F625W image is mapped onto the pre-SN WFPC2 images.

Figure 8 shows the 5″ × 5″ close-up of the SN 2006ov environment in the WFPC2 images. To guide the eye, white circles with a radius of 20 times the 1 σ uncertainty of the astrometric registration are marked. Within the very small 1 σ error circle, there is an apparent source in the F814W image, which we identify as the progenitor of SN 2006ov. A hint of this source can also be seen in the F606W image, although it appears somewhat extended. There are also some faint sources near the center of the error circle in the F450W image, but they appear to be offset from the progenitor in the F814W image. A bright source is seen to the northeast of the progenitor in all three bands. It looks stellar in the F814W image, but is somewhat extended in the F606W and F450W images, perhaps due to blending with another source. It is also possible that the source is actually a small star cluster. The presence of this bright source complicates the analysis of the photometry of the progenitor of SN 2006ov, as we further discuss in § 4.

In the pre-SN *HST* WFPC2 F450W and F814W images, the SN site is located at $(X, Y) = (571.62, 236.22)$ on Chip 4 (WFC4), with a 1 σ error circle of 0.17 pixel. In the F606W image, it is at $(X, Y) = (227.44, 267.34)$ on Chip 4 (WFC4), with a 1 σ error circle of 0.16 pixel. In the HSTphot coordinate system, these positions are $(X, Y) = (571.12, 235.72)$ for the F450W and F814W images and $(X, Y) = (226.94, 266.84)$ for the F606W image.

4. THE NATURE OF THE PROGENITORS OF SN 2006my AND SN 2006ov

We have identified the likely progenitors of SNe 2006my and 2006ov in pre-SN *HST* WFPC2 images. In this section, we study the nature of these objects based on their magnitudes and colors.

4.1. *Photometry of the Supernova Progenitors*

We used the software package HSTphot (Dolphin 2000a, 2000b) to conduct photometry of the *HST* WFPC2 images of SNe 2006my and 2006ov. HSTphot automatically accounts for

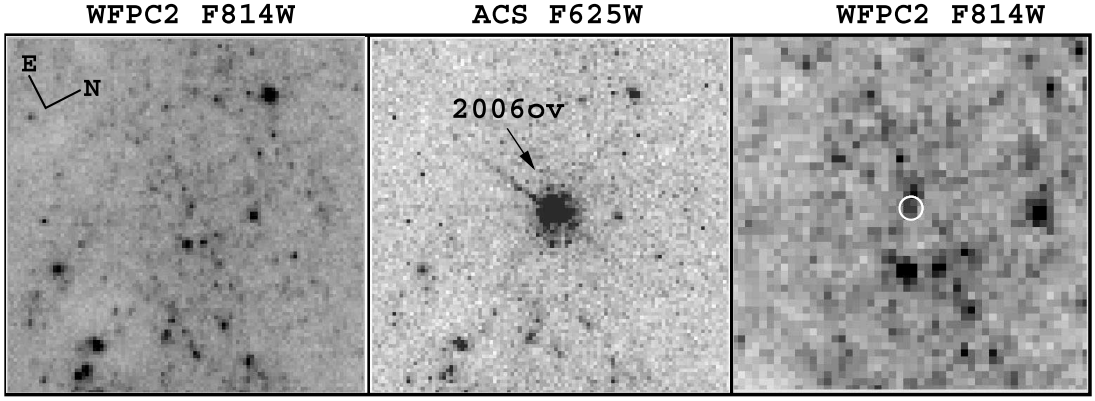

Fig. 7.—*Left:* A 10″ × 10″ section of the pre-SN *HST* WFPC2 F814W image of the SN 2006ov region. *Center*: A 10″ × 10″ section of the *HST* ACS F625W image with SN 2006ov, carefully registered to the image shown in the left panel. *Right:* A 5″ × 5″ close-up of the SN 2006ov environment. The white circle marks 10 times the 1 σ uncertainty of the astrometric registration. An apparent stellar object is seen in the center of the circle, although it is contaminated by a nearby bright source.

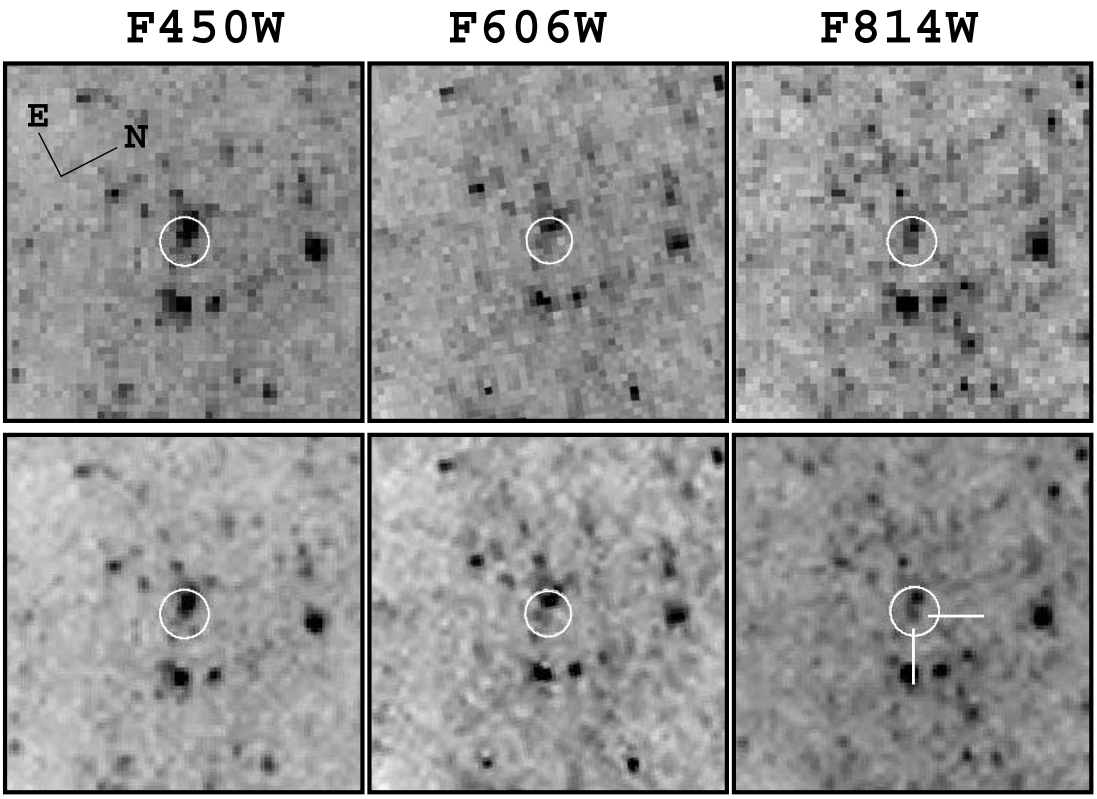

FIG. 8.—A $5'' \times 5''$ close-up of the SN 2006ov environment in the *HST* WFPC2 F450W, F606W, and F814W images. The white circles mark 20 times the 1 σ uncertainty of the astrometric registration. The F606W image is rotated to match the orientation of the F450W and F814W images. The top panel shows the images in the original WFPC2 resolution ($0.1''$ pixel^{-1}), while the bottom panel resamples the data to a resolution of $0.05''$ pixel^{-1} to bring out more details. The candidate progenitor is marked by a cross hair in the resampled F814W image. Photometry of the stars was performed on the original images.

WFPC2 PSF variations and charge-transfer effects across the chips, zero points, aperture corrections, etc. There are many option flags to run HSTphot. For our reduction, we chose to include Option 2 (turn on local sky determination) as recommended by the HSTphot manual for images of galaxies well beyond the Local Group, and Option 8 (turn off aperture corrections) as there are no good aperture correction stars in our images. HSTphot then uses the default aperture corrections for the filters, which are probably accurate in general to 0.02 mag. We also used an independent detection threshold of 2.5 σ (minimum S/N for a given image or filter for star detection), and a total detection threshold of 3.0 σ (minimum total S/N for a star to be kept in the final output). All photometry was performed on the co-added images in each filter.

Table 6 lists the HSTphot photometry for the progenitors of SNe 2006my and 2006ov. Columns (2) and (3) list the SN location as predicted by the astrometric solutions (§ 3). Columns (4) and (5) list the coordinates of the detected sources near the SN location in HSTphot. From the magnitudes of all 3 σ detections in the images, we also empirically determined the limiting magnitude near the SN sites in the images, and listed them in column (9) (Lmag) of Table 6. These limiting magnitudes are different ($\sim$0.5 to 1.0 mag shallower) from the values calculated with the WFPC2 ETC on the *HST* Web site,[9] as the SN sites are located on a bright stellar background.

[9] See http://www.stsci.edu/hst/wfpc2/software/wfpc2-etc.html.

TABLE 6
HSTPHOT PHOTOMETRY FOR THE PROGENITORS OF SNe 2006my AND 2006ov

SN (1)	X(p)[a] (2)	Y(p)[a] (3)	X(m)[b] (4)	Y(m)[b] (5)	S/N (6)	Mag1[c] (7)	Mag2[c] (8)	Lmag[d] (9)
2006my	410.11	158.31	409.72	158.13	5.6	F814W = 24.47(20)	I = 24.45(20)	I < 25.5
2006my	410.11	158.31	...	...	...	F555W < 26.5	V < 26.5	V < 26.5
2006ov	571.12	235.72	571.12[e]	235.72[e]	6.1	F814W = 23.19(18)	I = 23.08(18)	I < 24.6
2006ov	226.94	266.84	226.94[e]	266.84[e]	2.2	F606W = 24.07(50)	V = 24.24(50)	V < 25.3
2006ov	571.12	235.72	571.12[e]	235.72[e]	6.1[f]	F450W = 23.51(18)[f]	B = 23.40(18)[f]	B < 25.3

[a] The coordinates as predicted from the astrometric solutions.
[b] The coordinates as measured in HSTphot.
[c] Uncertainties in the last two digits for the magnitudes are indicated in parentheses.
[d] The 3 σ limiting magnitude. See text for details.
[e] The coordinates as enforced in HSTphot. See text for details.
[f] This detection is likely caused by another source and not the progenitor of SN 2006ov. See text for details.

For SN 2006my in NGC 4651, HSTphot detected a 5.6 σ source close to ($\lesssim$0.43 pixel), and within the 1 σ error of, the predicted SN location in the F814W image, with a flight system magnitude of F814W = 24.47 $\pm$ 0.20. For the F555W image, HSTphot failed to detect any source within the 1 σ error radius (the closest detection is an extended source near the $\sim$2 σ error radius). Inspection of Figure 5 indicates that there is no apparent point source within the 1 σ error radius. As HSTphot has an option to accept predetermined star lists, we enforced HSTphot to make a measurement at the position of the progenitor as measured by HSTphot in the F814W image; this yielded a 2.2 σ detection with a flight system magnitude of F555W = 26.66 $\pm$ 0.55. As this F555W magnitude is fainter than the 3 σ limit (F555W $<$ 26.5 mag) of the image, we consider the progenitor to be not detected in the F555W image, and use the 3 σ limiting magnitude (V $<$ 26.5 mag) as the upper limit for the V-band flux of the progenitor.

For SN 2006ov in M61, HSTphot failed to detect any sources within the 1 σ error radius of the SN location in the F814W image. Lowering the total detection threshold to 2 σ did not help. Inspection of the residual image generated by HSTphot after subtracting the PSFs of all positive detections, however, reveals an apparent source close to the known SN location. Contamination by the bright source to the northeast of the SN location is a possible explanation for the failure by HSTphot to make a detection of the central source in the error circle.

Since we have an accurate (1 σ = 0.17 pixel) position for the putative progenitor of SN 2006ov as determined from the ACS/HRC to WFPC2 astrometric registration, we forced HSTphot to make a measurement at the progenitor position. This procedure yielded a 6.1 σ detection with F814W = 23.19 $\pm$ 0.18 mag, and a residual image with all sources within the 1 σ error radius cleanly removed. We further forced HSTphot to make a measurement at the progenitor position in the F450W and F606W images. We measured a 2.2 σ source with F606W = 24.07 $\pm$ 0.50, and a 6.1 σ source with F450W = 23.51 $\pm$ 0.18 mag. Although the detection in the F606W image is of low S/N (2.2 σ) due to possible blending from other sources, the measured magnitude (F606W = 24.07 $\pm$ 0.50 mag) is brighter than the 3 σ limiting magnitude (F606W $<$ 25.3 mag), and inspection of Figure 8 suggests a hint of the progenitor in the F606W image, so we kept the F606W detection as it is. The 6.1 σ detection in the F450W image is likely caused by another source; as previously noted, it appears to be offset from the progenitor in the F814W image. Moreover, if it were indeed the progenitor, then the spectral energy distribution would be unrealistic, with a red $V - I$ color and a blue $B - V$ color. We assume that, because of the spatial offset, this blue source does not substantially affect our V and I measurements of the putative progenitor, although there might be some contamination.

The flight-system magnitudes were then transformed to the standard broadband *BVRI* system following the prescriptions by Holtzman et al. (1995) and Dolphin (2000b), and are listed in column (8) (Mag2) of Table 6.

4.2. *Properties of the Supernova Progenitors*

We can estimate the masses of the progenitor stars by comparing the intrinsic colors and absolute magnitudes of the objects with stellar evolution tracks of massive stars having different zero-age main-sequence masses ($M_{\rm zams}$). In § 4.1 we measured the apparent magnitudes of the possible progenitors (see Table 6 for a summary). To estimate the absolute magnitudes of the progenitors, we need to know the distances to NGC 4651 and M61.

For NGC 4651, Solanes et al. (2002) collected seven distance measurements derived by different groups using the Tully-Fisher (T-F) method, and reported an average distance modulus of μ = 31.74 $\pm$ 0.25 mag. Terry et al. (2002) reported a "sosie galaxy" T-F distance of μ = 31.86 $\pm$ 0.17 mag. We adopt μ = 31.8 $\pm$ 0.3 mag as a possible distance to NGC 4651.

For M61, the T-F distance published by Tully (1988) is μ = 30.91 mag, while Schöniger & Sofue (1997) reported a CO and H I T-F distance of μ = 30.12 $\pm$ 0.10 mag. We adopt μ = 30.5 $\pm$ 0.4 mag as a possible distance to M61.

Both NGC 4651 and M61 may be members of the Virgo Cluster (VC), one of the nearest rich clusters in the northern hemisphere with over 1300 member galaxies, so we also attempted to use the measured distance to the VC as the distance of both NGC 4651 and M61. The VC, however, is quite extended in size and has complicated three-dimensional structure. The two main components are the somewhat more nearby, northern, M87 subcluster (dominated by early-type galaxies), and the somewhat more distant, southern, M49 galaxy concentration (rich in spiral galaxies). Currently, there is a total of eight VC spiral galaxies with Cepheid distances (NGC 4496A, NGC 4536, NGC 4548, NGC 4321, NGC 4535, NGC 4639, NGC 4527, NGC 4414; see the summary by Freedman et al. 2001), and their average distance is μ = 31.03 $\pm$ 0.12 mag. A recent B-band T-F distance measurement to 51 VC spiral galaxies yields μ = 31.28 $\pm$ 0.14 mag (Fouqué et al. 2001). Two recent surface brightness fluctuation (SBF) measurements to the elliptical galaxies in the VC yield μ = 31.09 $\pm$ 0.15 mag (Tonry et al. 2001; Jerjen et al. 2004). The distance to the VC galaxy IC 3338 using the tip of the red giant branch (TRGB) method gives μ = 30.98 $\pm$ 0.19 mag (Harris 1998). Here we adopt μ = 31.1 $\pm$ 0.2 mag as the average distance to VC. To account for the line-of-sight diameter of the VC, we further adopt μ = 31.1 $\pm$ 0.5 mag as another possible distance to both NGC 4651 and M61.

We also note that NGC 4651 is $\sim$4° north of the M87 subcluster, while M61 is $\sim$8° south of the M87 subcluster (and thus possibly a member of the M49 subcluster). At face value, our adopted individual distances of NGC 4651 and M61 (μ = 31.8 $\pm$ 0.3 and 30.5 $\pm$ 0.4 mag, respectively) contradict the depicted structure of the VC: NGC 4651 is in the more nearby northern region, but it has a larger adopted distance than the average VC; M61 is in the more distance southern subcluster, but it has a smaller adopted distance than the average VC. As discussed by Pilyugin et al. (2004), however, it seems impossible to check the distance of individual VC galaxies by comparing their value with the "group" distance, largely because of the complicated three-dimensional structure of the cluster.

The evolutionary tracks of massive stars on the color-magnitude diagrams (CMDs) are significantly affected by the adopted metallicity, so we attempt to constrain the metallicity of the sites of SNe 2006my and 2006ov by using information from the literature. From the CFHT images, we measured that SN 2006my is 27.4″ west and 22.1″ south of the nucleus of NGC 4651, and that SN 2006ov is 6.1″ east and 51.1″ north of the nucleus of M61. With these offsets, the galaxy position angle and the inclination angle from LEDA,[10] and the published metallicity and its radial gradient in NGC 4651 and M61 by Pilyugin et al. (2004), we derived the relative oxygen abundance log (O/H) + 12 = 8.51 $\pm$ 0.06 and 8.64 $\pm$ 0.10 dex for the sites of SN 2006my and SN 2006ov, respectively. These metallicities are lower than the solar value (8.8 dex; Grevesse & Sauval 1998), so we adopt a subsolar metallicity of Z = 0.008 for the environment of both SNe.

Figure 9 shows the $(V - I)^0$ versus M_I^0 CMD for the progenitor of SN 2006my in NGC 4651, compared with model stellar

[10] See http://leda.univ-lyon1.fr.

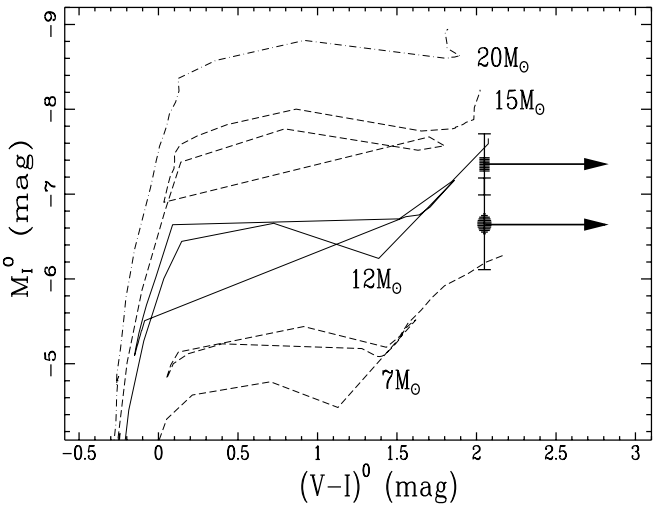

FIG. 9.—$(V-I)^0$ vs. M_I^0 color-magnitude diagram for the progenitor of SN 2006my. The filled square represents the data with an adopted distance modulus of $\mu = 31.8 \pm 0.3$ mag for SN 2006my, while the filled circle represents the data with $\mu = 31.1 \pm 0.5$ mag. Also shown are model stellar evolution tracks for a range of masses from Lejeune & Schaerer (2001), with enhanced mass loss for the most massive stars and a metallicity of $Z = 0.008$.

evolution tracks for a range of masses from Lejeune & Schaerer (2001), assuming enhanced mass loss for the most massive stars and a metallicity of $Z = 0.008$. We have corrected the magnitudes of the progenitor with the Galactic reddening only [$E(B-V) = 0.027$ mag], as discussed in § 2.2. The uncertainties in the photometry and the distance are added in quadrature to produce the final uncertainty for the absolute magnitude. As a result of only an upper limit to the brightness of the progenitor in the V band, we have a lower limit to the $(V-I)^0$ color, as illustrated by the arrows in Figure 9. The filled square represents the data with an adopted distance modulus of $\mu = 31.8 \pm 0.3$ mag. From the location of the progenitor on the CMD, $M_{\rm zams} = 11$–$15\ M_\odot$ is estimated. The filled circle represents the data when the average VC distance ($\mu = 31.1 \pm 0.5$ mag) is used, which suggests $M_{\rm zams} = 7$–$12\ M_\odot$.

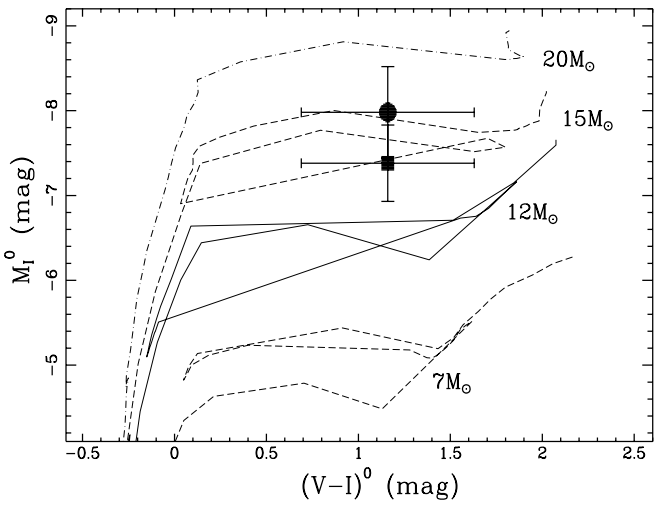

FIG. 10.—$(V-I)^0$ vs. M_I^0 color-magnitude diagram for the progenitor of SN 2006ov. The filled square represents the data with an adopted distance modulus of $\mu = 30.5 \pm 0.4$ mag for SN 2006ov, while the filled circle represents the data with $\mu = 31.1 \pm 0.5$ mag. Also shown are model stellar evolution tracks for a range of masses from Lejeune & Schaerer (2001), with enhanced mass loss for the most massive stars and a metallicity of $Z = 0.008$.

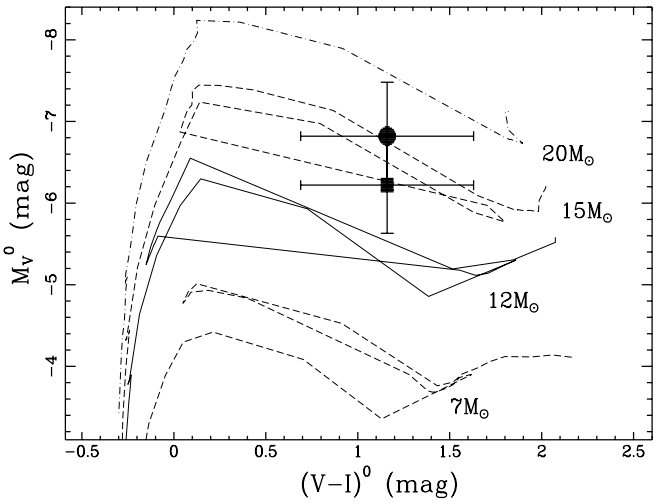

FIG. 11.—$(V-I)^0$ vs. M_V^0 color-magnitude diagram for the progenitor of SN 2006ov. The filled square represents the data with an adopted distance modulus of $\mu = 30.5 \pm 0.4$ mag for SN 2006ov, while the filled circle represents the data with $\mu = 31.1 \pm 0.5$ mag. Also shown are model stellar evolution tracks for a range of masses from Lejeune & Schaerer (2001), with enhanced mass loss for the most massive stars and a metallicity of $Z = 0.008$.

Figure 10 shows the $(V-I)^0$ versus M_I^0 CMD for the progenitor of SN 2006ov in M61, after correcting the magnitudes of the progenitor with the Galactic reddening of $E(B-V) = 0.022$ mag. Adopting $\mu = 30.5 \pm 0.4$ mag, the $M_{\rm zams}$ estimate for the progenitor is 13–17 $M_\odot$. With the average VC distance ($\mu = 31.1 \pm 0.5$ mag), we find $M_{\rm zams} = 15$–$19\ M_\odot$. Figure 11 shows the $(V-I)^0$ versus M_V^0 CMD for the same object. The $M_{\rm zams}$ estimate for the progenitor is 12–17 and 14–20 $M_\odot$ for our two choices of the distance, respectively.

It is clear that the adopted distances to the galaxies have a relatively large impact on the derived progenitor masses. As a by-product of the CMD study, we provide an independent constraint on the distances to NGC 4651 and NGC 4303 from the global stellar photometry on the *HST* images. For SN 2006my, we measured the photometry of all the stars (with S/N $\gtrsim 3$) on the four WFPC2 chips on the F555W and F814W images, and plotted their magnitudes on the $(V-I)^0$ versus M_I^0 CMD with an adopted distance to NGC 4651. The isochrones of the stellar evolutionary tracks from Lejeune & Schaerer (2001) are then plotted on the CMD to see whether they are a good fit to the data. Although this method is plagued by the need to adopt a global metallicity for all the stars (while in reality they should come from a range of metallicities from different regions of NGC 4651), possible contamination of compact stellar clusters in the photometry, and no reddening corrections, it nevertheless suggests that $\mu = 31.1 \pm 0.5$ mag (the average VC distance) provides a better fit to the data than the average T-F distances ($\mu = 31.8 \pm 0.3$). For SN 2006ov, the F450W and F814W images were used to derive a $(B-I)^0$ versus M_I^0 CMD, and the data favor the average T-F distance ($\mu = 30.5 \pm 0.4$ mag) over the average VC distance ($\mu = 31.1 \pm 0.5$ mag). The global metallicity was adopted as solar for both galaxies, even though the SN sites are subsolar.

Owing to the relatively large uncertainties in the distance estimates, our conservative approach is to adopt the progenitor masses as derived from the distances favored by the CMD study ($\mu = 31.1 \pm 0.5$ mag for SN 2006my, and $\mu = 30.5 \pm 0.4$ mag for SN 2006ov), but allow the error bars to cover the range of progenitor masses from the other distance estimate. This gives $M_{\rm zams} = 10^{+5}_{-3}\ M_\odot$ for the progenitor of SN 2006my in NGC 4651, and $15^{+5}_{-3}\ M_\odot$ for the progenitor of SN 2006ov in M61. Both

TABLE 7
Masses and Mass Limits for the Progenitors of Core-Collapse SNe

SN	SN type	Progenitor mass ($M_\odot$)	Progenitor Mass Limit	References
1987A	II-peculiar	~20		1, 2
1993J	IIb	~17		3, 4
1999ev	II-P	15–18		5
2003gd	II-P	6–12		6, 7
2004A	II-P	7–12		8
2004et	II-P	13–20		9
2005cs	II-P	7–13		10, 11
2006my	II-P	7–15		This paper
2006ov	II-P	12–20		This paper
2005gl	IIn? II-L?		40–80 $M_\odot$ LBV? CSC?	12
2004dj	II-P		~12–15 $M_\odot$? >20 $M_\odot$? (in CSC)	13, 14, 15
1999em	II-P		$\lesssim$15 $M_\odot$	16
1999gi	II-P		$\lesssim$12–20 $M_\odot$	17
2001du	II-P		$\lesssim$9–21 $M_\odot$	16, 18
1999an	II-P		$\lesssim$20 $M_\odot$	5
1999br	II-P		$\lesssim$12 $M_\odot$	5
2000ds	Ib/c		$\lesssim$7 $M_\odot$ RSG? WR?	5
2000ew	Ib/c		Low-mass RSG; WR?	5
2001B	Ib/c		$\lesssim$25 $M_\odot$ RSG? WR?	5
2004gt	Ib/c		~20–40 $M_\odot$? WR?	19, 20

References.—(1) Gilmozzi et al. 1987; (2) Sonneborn et al. 1987; (3) Aldering et al. 1994; (4) Van Dyk et al. 2002; (5) Maund & Smartt 2005; (6) Van Dyk et al. 2003c; (7) Smartt et al. 2004; (8) Hendry et al. 2006; (9) Li et al. 2005b; (10) Li et al. 2006; (11) Maund et al. 2005a; (12) Gal-Yam et al. 2007; (13) Wang et al. 2005; (14) Maíz-Apellániz et al. 2004; (15) Vinkó et al. 2006; (16) Smartt et al. 2003; (17) Leonard et al. 2002a; (18) Van Dyk et al. 2003b; (19) Gal-Yam et al. 2005; (20) Maund et al. 2005b.

progenitors have a red color, albeit with a large uncertainty. Their locations on the CMDs suggest that the progenitor of SN 2006my is a RSG, while the progenitor of SN 2006ov is consistent with either a RSG or a YSG.

5. DISCUSSION

5.1. *Progenitors of SN 2006my and SN 2006ov*

We have located the sites of SNe 2006my and 2006ov to high precision on pre-SN *HST* WFPC2 images, and identified the likely progenitor stars of both SNe. As can be seen in Figures 1 and 2, both SNe occurred on a spiral arm of their host galaxies, and their immediate environments are heavily contaminated by host-galaxy emission (more so for SN 2006ov than SN 2006my). Even at *HST* WFPC2 resolution (Figs. 5 and 8), there are many sources in the SN environments. It is thus possible that the objects we identified in the error circles are just RSGs that happened to be close to the SN explosion, but are completely unrelated.

The confidence of the progenitor identifications can be strengthened if we put stringent limits on the nondetection of the progenitors. Using the limiting magnitudes in Table 5, we place the following mass limits if the progenitors of SNe 2006my and 2006ov were not detected in the *HST* WFPC2 F814W images: $M_{\rm zams} \lesssim 11$ or 8 $M_\odot$ for the SN 2006my progenitor, when $\mu = 31.8 \pm 0.3$ and $\mu = 31.1 \pm 0.5$ mag are adopted for NGC 4651, respectively; $M_{\rm zams} \lesssim 9$ or 13 $M_\odot$ for the SN 2006ov progenitor, when $\mu = 30.5 \pm 0.4$ and $\mu = 31.1 \pm 0.5$ mag are adopted for M61, respectively. These mass limits are not very restrictive, unfortunately, as several of the previously identified progenitors for SNe II-P have masses in the range 8–13 $M_\odot$ (Van Dyk et al. 2003a; Smartt et al. 2004; Maund et al. 2005a; Li et al. 2006; Hendry et al. 2006). Hence, there exists the possibility that the progenitors of SN 2006my and/or SN 2006ov were not detected.

The probability of a chance coincidence (that is, the objects we identified are unrelated RSGs that happened to be within the error circles) can be further assessed by studying the density of RSGs in the SN environments. Within a 1.0″ radius (approximately 80 pc at our adopted average VC distance), we identified six possible RSGs (eight possible RSGs) in the neighborhood of SN 2006my (SN 2006ov) by noting their absolute magnitudes and colors on the CMDs. The probability of a RSG within the 0.045″ (0.02″) error radius is thus 1.2% (0.2%). The small probability (0.2%) of a chance coincidence for the progenitor of SN 2006ov solidifies our identification. While the probability of a chance coincidence for the progenitor of SN 2006my is also small (1.2%), the confidence of our progenitor identification can be further increased if we can significantly reduce the astrometric error radius.

In § 3.1 we also mentioned a possible blending issue for the progenitor of SN 2006my. Using the RSG density in the environment of SN 2006my, the chance of two RSGs occurring in adjacent WFC pixels (0.1″) is only 0.4%, assuming that massive stars do not tend to occur in clusters. (The probability of blending would increase somewhat if the tendency of massive stars to occur in associations were included, but it would still likely be relatively low.)

The two main reasons for the large mass range of our identified progenitors are (1) the uncertain distances to the galaxies, and (2) the large photometric uncertainty due to the low S/N of the detections. When more accurate distances for the galaxies (e.g., Cepheid distances) become available, the masses of the progenitors will be further constrained. The second problem highlights the difficulty in directly identifying progenitors of SNe: they are faint beyond the Local Group, and the pre-SN *HST* archival images often do not have the optimal combination of filters and depth because most of them were obtained by various observers for different projects. A dedicated *HST* program to

image the most nearby galaxies would give observers a chance to identify the progenitors of most core-collapse SNe in these galaxies, further advancing our understanding of the death of massive stars.

5.2. *The Nature of Core-Collapse Supernova Progenitors*

Our identified progenitors of SN 2006my and SN 2006ov increase the number of directly detected progenitors for genuine SNe from 7 to 9. The first half of Table 7 lists the inferred masses of these progenitors. The progenitors of several probable superoutbursts of luminous blue variables (LBVs) misclassified as SNe, such as SN 1961V (Zwicky 1964) and SN 1997bs (Van Dyk et al. 1999, 2000), have been identified but are not listed.

The second half of Table 7 gives the mass limits for the progenitors of several core-collapse SNe. For these SNe, the progenitors are not directly identified, but a mass limit is derived based on the limiting magnitudes of pre-SN images. In particular, SN 2004dj occurred in a compact star cluster (CSC), and the mass of the progenitor is estimated from the properties (luminosity and color) of the CSC (Maíz-Apellániz et al. 2004; Wang et al. 2005). SN 2005gl is associated with a very luminous ($M_V = -10.3 \pm 0.2$ mag) source (Gal-Yam et al. 2007), which could be a very massive single star (e.g., an LBV) or a CSC. There is also some uncertainty regarding the exact type of the SN: while a very early-time spectrum showed narrow hydrogen lines typical of SNe IIn, its later spectral evolution is more typical of normal SNe II, perhaps a SN II-L.

It is clear from Table 7 that observers have had the most success identifying progenitors for SNe II-P (seven of nine). The main reason for this is perhaps the relative frequency of different types of SNe. A preliminary analysis indicates that out of the 68 core-collapse SNe discovered by LOSS within 30 Mpc in the past 9 years, 46 are SNe II (most of which are SNe II-P), 18 are SNe Ib/c, 1 is a SN IIb, and 3 are SNe IIn. SNe II-P are thus by far the most common type of core-collapse SN. Still, it is a bit surprising that no direct progenitor has been detected for a SN Ib/c, given that they are roughly 40% as frequent as SNe II from the LOSS statistics. One factor is perhaps the low luminosity of the possible progenitors for SNe Ib/c, which also limits the progenitors to be either relatively low-mass stripped stars in binary systems, or single Wolf-Rayet stars.

The inferred masses for the progenitors of SNe 2006my and 2006ov are consistent with the trend that SNe II-P come from low-mass (8–20 $M_\odot$) RSGs, as previously suggested (Li et al. 2006; Hendry et al. 2006). In total, there are now seven directly identified progenitors for SNe II-P, all with $M_{\rm zams} \lesssim 20\ M_\odot$. The statistics are growing, and they suggest that perhaps all SNe II-P come from low-mass RSGs. If this is true, stars more massive than $\sim 20\ M_\odot$ may have a different evolutionary path and explode as other types of SNe such as SNe II-L or SNe IIn. The possible association of the SN IIn/II-L 2005gl with a very massive single star (Gal-Yam et al. 2007) is in agreement with this speculation. In the future, when a very massive star explodes as a SN in a nearby galaxy (a rare event), observers may have a chance to study both the massive star and the SN in detail. Until then, the fate of the very massive stars ($M_{\rm zams} > 20\ M_\odot$) still needs to be observationally verified.

6. CONCLUSIONS

Our main conclusions are the following:

1. Both SN 2006my in NGC 4651 and SN 2006ov in M61 are SNe II-P discovered 3–4 months after explosion. Their spectra show no evidence of strong host-galaxy reddening.
2. We obtained high-quality ground-based CFHT images for both SNe, and were able to locate the SN sites to high precision on the pre-SN *HST* WFPC2 images (astrometric uncertainty $1\ \sigma = 0.045''$ and $0.11''$ for SNe 2006my and 2006ov, respectively). We further improved the astrometric solution to $1\ \sigma = 0.02''$ for SN 2006ov with *HST* ACS images of the SN. Within each error circle, we identified a likely progenitor of each SN.
3. Photometric analysis suggests that the progenitor of SN 2006my has $M_{\rm zams} = 10^{+5}_{-3}\ M_\odot$, and the progenitor for SN 2006ov has $M_{\rm zams} = 15^{+5}_{-3}\ M_\odot$. There is a small probability (1.2% and 0.2%, respectively) that the object we identified as the progenitor is caused by chance coincidence.
4. The inferred masses for the possible progenitors of SNe 2006my and 2006ov are consistent with the trend that the most common core-collapse SNe II-P arise from stars with $M_{\rm zams}$ in the range 8–20 $M_\odot$.

We thank Louis Desroches, Mohan Ganeshalingam, Jennifer Hoffman, Douglas Leonard, Frank Serduke, Jeffery Silverman, and Diane Wong for obtaining and reducing the optical spectra of SNe used in this paper with the 3 m Shane reflector at Lick Observatory. The work of A. V. F.'s group at U. C. Berkeley is supported by National Science Foundation grant AST 06-07485, and by the TABASGO Foundation. Additional funding is provided by NASA through grants AR-10690, AR-10952, and GO-10877 from the Space Telescope Science Institute, which is operated by the Association of Universities for Research in Astronomy, Inc., under NASA contract NAS 5-26555. KAIT was made possible by generous donations from Sun Microsystems, Inc., the Hewlett-Packard Company, AutoScope Corporation, Lick Observatory, the National Science Foundation, the University of California, and the Sylvia and Jim Katzman Foundation.

REFERENCES

Aldering, G., Humphreys, R. M., & Richmond, M. W. 1994, AJ, 107, 662
Bessell, M. S. 1999, PASP, 111, 1426
Blondin, S., Modjaz, M., Kirshner, R., Challis, P, & Berlind, P. 2006, CBET, 757, 1
Dolphin, A. E. 2000a, PASP, 112, 1383
———. 2000b, PASP, 112, 1397
Elmhamdi, A., et al. 2003, MNRAS, 338, 939
Filippenko, A. V. 1988, AJ, 96, 1941
———. 1997, ARA&A, 35, 309
———. 2005, in ASP Conf. Ser. 332, The Fate of the Most Massive Stars, ed. R. Humphreys & K. Stanek (San Francisco: ASP), 33
Filippenko, A. V., Li, W., Treffers, R. R., & Modjaz, M. 2001, in ASP Conf. Ser. 246, Small-Telescope Astronomy on Global Scales, ed. W.-P. Chen, C. Lemme, & B. Paczyński (San Francisco: ASP), 121
Filippenko, A. V., Matheson, T., & Ho, L. C. 1993, ApJ, 415, L103
Foley, R. J., et al. 2003, PASP, 115, 1220
Fouqué, P., Solanes, J. M., Sanchis, T., & Balkowski, C. 2001, A&A, 375, 770
Freedman, W. L., et al. 2001, ApJ, 553, 47
Gal-Yam, A., et al. 2005, ApJ, 630, L29
———. 2007, ApJ, 656, 372
Gilmozzi, R., et al. 1987, Nature, 328, 318
Grevesse, N., & Sauval, A. J. 1998, Space Sci. Rev., 85, 161
Hamuy, M. 2003, ApJ, 582, 905
Hamuy, M., et al. 2001, ApJ, 558, 615
Harris, W. E. 1998, Nature, 395, 45
Hendry, M. A., et al. 2005, MNRAS, 359, 906
———. 2006, MNRAS, 369, 1303
Holtzman, J. A., et al. 1995, PASP, 107, 1065
Jerjen, H., Binggeli, B., & Barazza, F. D. 2004, AJ, 127, 771
Lejeune, T., & Schaerer, D. 2001, A&A, 366, 538

Leonard, D. C., et al. 2002a, AJ, 124, 2490
———. 2002b, PASP, 114, 35
Li, W., Filippenko, A. V., Chornock, R., & Jha, S. 2003, ApJ, 586, L9
Li, W., Filippenko, A. V., & Van Dyk, S. D. 2005a, Astron. Tel., 492, 1
Li, W., Van Dyk, S. D., Filippenko, A. V., & Cuillandre, J.-C. 2005b, PASP, 117, 121
Li, W., et al. 2000, in Cosmic Explosions, ed. S. S. Holt & W. W. Zhang (Melville: AIP), 103
———. 2006, ApJ, 641, 1060
Maíz-Apellániz, J., Bond, H. E., Siegel, M. H., Lipkin, Y., Maoz, D., Ofek, E. O., & Poznanski, D. 2004, ApJ, 615, L113
Matheson, T. 2000, Ph.D. thesis, Univ. California (Berkeley)
Maund, J. R., & Smartt, S. J. 2005, MNRAS, 360, 288
Maund, J. R., Smartt, S. J., & Danziger, I. J. 2005a, MNRAS, 364, L33
Maund, J. R., Smartt, S. J., & Schweizer, F. 2005b, ApJ, 630, L33
Miller, J. S., & Stone, R. P. S. 1993, Lick Obs. Tech. Rep. No. 66
Nakano, S., & Itagaki, K. 2006a, CBET, 727, 1
———. 2006b, CBET, 756, 1
Nomoto, K., Suzuki, T., Shigeyama, T., Kumagai, S., Yamaoka, H., & Saio, H. 1993, Nature, 364, 507
Oke, J. B., et al. 1995, PASP, 107, 375
Pastorello, A., et al. 2006, MNRAS, 370, 1752
Pilyugin, L. S., Vílchez, J. M., & Contini, T. 2004, A&A, 425, 849
Schlegel, D. J., Finkbeiner, D. P., & Davis, M. 1998, ApJ, 500, 525
Schöniger, F., & Sofue, Y. 1997, A&A, 323, 14
Smartt, S. J., Maund, J. R., Hendry, M. A., Tout, C. A., Gilmore, G. F., Mattila, S., & Benn, C. R. 2004, Science, 303, 499
Smartt, S. J., et al. 2003, MNRAS, 343, 735
Solanes, J. M., Sanchis, T., Salvador-Solé, E., Giovanelli, R., & Haynes, M. P. 2002, AJ, 124, 2440
Sonneborn, G., Altner, B., & Kirshner, R. P. 1987, ApJ, 323, L35
Stanishev, V., & Nielsen, T. B. 2006, CBET 737, 1
Stetson, P. B. 1987, PASP, 99, 191
Takáts, K., & Vinkó, J. 2006, MNRAS, 372, 1735
Terry, J. N., Paturel, G., & Ekholm, T. 2002, A&A, 393, 57
Tonry, J., et al. 2001, ApJ, 546, 681
Tully, R. B. 1988, Nearby Galaxies Catalogue (Cambridge: Cambridge Univ. Press)
Van Dyk, S. D., Garnavich, P. M., Filippenko, A. V., Höflich, P., Kirshner, R. P., Kurucz, R. L., & Challis, P. 2002, PASP, 114, 1322
Van Dyk, S. D., Li, W., & Filippenko, A. V. 2003a, PASP, 115, 1
———. 2003b, PASP, 115, 448
———. 2003c, PASP, 115, 1289
Van Dyk, S. D., Peng, C. Y., Barth, A. J., & Filippenko, A. V. 1999, AJ, 118, 2331
Van Dyk, S. D., Peng, C. Y., King, J. Y., Filippenko, A. V., Treffers, R. R., Li, W. D., & Richmond, M. W. 2000, PASP, 112, 1532
Vinkó, J., et al. 2006, MNRAS, 369, 1780
Wang, X., Yang, Y., Zhang, T., Ma, J., Zhou, X., Li, W., Lou, Y., & Li, Z. 2005, ApJ, 626, L89
Zhang, T., Wang, X., Li. W., Zhou, X., Ma, J., Jiang, Z., & Chen, J. 2006, AJ, 131, 2245
Zwicky, F. 1964, ApJ, 139, 514